Fibre Orientation Modelling for Rubber Press Forming of Thermoplastic Laminates

E.A.D. Lamers, R. Akkerman & S. Wijskamp

University of Twente
Department of Mechanical Engineering
Composites Group
PO box 217
7500 AE Enschede
the Netherlands

URL: www.composites.ctw.utwente.nl
E.A.D.Lamers@ctw.utwente.nl
R.Akkerman@ctw.utwente.nl
S.Wijskamp@ctw.utwente.nl

ABSTRACT: *The fibre re-orientation caused by the press forming of thermoplastic composites is one of the main factors in the process induced product distortions. Classical geometric drape simulation methods can be used to predict this fibre re-orientation. However, these methods have difficulties to incorporate the process specific boundary conditions. Therefore, a fabric reinforced fluid model was implemented into the Finite Element package DIEKA, which is capable of modelling the boundary conditions as well. The predictions of both types of simulations are compared with the results of drape experiments on a double dome geometry.*

KEY WORDS: *composites, draping, FE-draping, material forming*

1. Introduction

Thermoplastic composites have a good potential to improve the cost-effectiveness of advanced polymer composites. Hot pressing of these materials offers a significantly higher production rate than using the autoclave processes, increasing the economical competitiveness to other construction materials such as for example aluminium.

A relatively fast process is the Rubber Press Forming process (RPF) for fabric-reinforced thermoplastics. Typically, the production cycle is in the order of a few minutes and consists of infrared heating of a multi-layer preform above its melt or glass transition temperature, hot pressing of the preform and cooling the product below the solidification temperature of the thermoplastic matrix.

In the process, the negatively shaped rubber upper mould presses the hot preform on a positively shaped steel lower mould. During pressing the rubber deforms nearly hydrostatically, proving a good way to consolidate the laminate.

Heating, pressing, cooling and removing the product from the press are automated, ensuring reproducibility. Due to the good draping characteristics of the fabric material, the processing forces are low and the tools are relatively inexpensive.

However, during production shrinkage and warpage may result in unacceptable dimensional changes of the products. Fibre re-orientation is one of the major factors causing these distortions. Especially when producing doubly curved parts, the process of draping causes the angle between the warp and weft yarns to vary over the product. As a result of this re-orientation, the thermomechanical properties of the fibre reinforced composite material show a corresponding distribution, in turn leading to a distribution of residual stresses. Obviously, the resulting fibre orientations must be predicted accurately to predict the overall thermomechanical properties and distortions of the product.

In the past, draping has been modelled using several methods. A widely used method is geometrical draping. Geometrical draping methods are, however, nearly incapable of modelling process specific boundary conditions. Finite Element (FE) simulations are used to predict the fibre re-orientation incorporating these conditions.

Here, an extension to the fabric reinforced fluid model (Spencer 2000) was implemented into DIEKA, an FE package used for modelling forming processes, such as e.g. deep drawing of metals (Meinders *et al.*, 1997). Using different lay-ups, drape experiments were performed on a double dome geometry. Finally, the FE-model and the geometrical draping method are compared with experimental results.

2. Geometrical Draping

The geometrical draping approach is commonly used to predict the resulting fibre re-orientation for doubly curved fabric reinforced products. Based on a pin-

joint description of the weave, this model was initially described by Mack and Taylor (Mack *et al.*, 1956), and more recently by Robertson, Hsiue and Yeh (Robertson *et al.*, 1984) and Bergsma (Bergsma 1995). The model assumes inextensible fibres pinned together at their crossings, allowing free rotation at these joints.

Typically, draping starts from an initial point and two initial fibre directions. Further points are then generated at a fixed equal distance from the previous points. By applying certain "strategies" (Bergsma 1995), different drape solutions can be found.

The method is nearly incapable of incorporating the processing conditions during draping and accurate representation of the composite properties. Especially in tight weaves, the error of assuming a zero in-plane fabric shear stiffness during draping leads to errors in predicting the resulting fibre distribution. The resin material also affects the deformation properties. Inaccurate drape predictions can be obtained with products where bridging occurs or when the preform slides over the mould during forming. In addition, the geometrical approach might find infeasible solutions when draping products with holes.

3. Finite Element Draping

The incapabilities of the geometrical draping method are resolved by using FE methods, as demonstrated by several authors (Boisse *et al.*, 1997, De Luca *et al.*, 1998 and McEntee *et al.*, 1998). Here, a drape material model is developed, based on a continuum description of motion, and implemented into an implicit updated Lagrangian FE package.

3.1. *Material model*

The drape material constitutive equation derived here is an extension to the fabric reinforced fluid model by Spencer (Spencer 2000). The composite components, the two fibre families and the resin, are subjected to an affine deformation (see figure 1). Thus, similarly to parallel spring-damper models, the stress $\underline{\sigma}$ can be split into two parts or:

$$\underline{\sigma} = \underline{\sigma}_e + \underline{\tau}\,, \qquad [1]$$

where $\underline{\sigma}_e$ is the elastic stress contribution and $\underline{\tau}$ is an extra viscous stress contribution. The elastic and viscous contributions to the stress are solved separately, allowing a description of the complex fabric behaviour such as the phenomenon of locking.

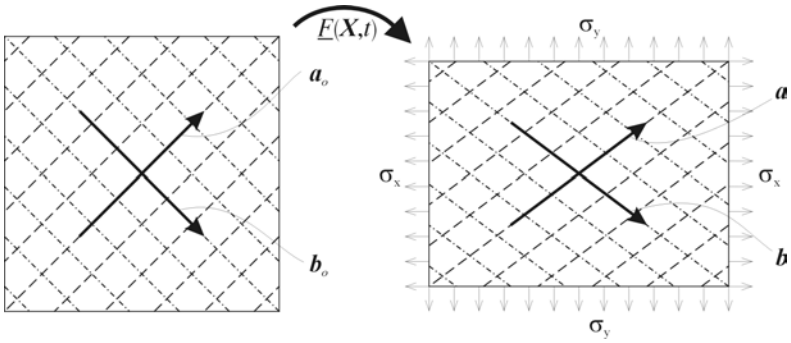

Figure 1. *Affine deformation of fibres and resin*

In figure 1, $\boldsymbol{a}$ and $\boldsymbol{b}$ are vectors, representing the two fibre families of the fabric, $\varphi(\boldsymbol{X},t)$ relates the original configuration to the current configuration in time and $\sigma_{x,y}$ are the stresses in x and y direction respectively.

3.1.1. Elastic stress contribution

The elastic stress $\underline{\sigma}_e$ is split as:

$$\underline{\sigma}_e = \underline{\sigma}_p + \underline{\sigma}_a + \underline{\sigma}_b + \underline{\sigma}_f \,, \qquad [2]$$

where $\underline{\sigma}_p$ is the hydrostatic pressure, $\underline{\sigma}_{a,b}$ the elastic contributions of the fibre families a and b and $\underline{\sigma}_f$ is the elastic contribution of the fabric itself, caused by the interaction of the two fibre families.

Assuming a continuous distribution of the fibres, the two fibre families of the fabric can be described with two vectors $\boldsymbol{a}(\boldsymbol{X}, t)$ and $\boldsymbol{b}(\boldsymbol{X}, t)$ which can vary spatially and in time, or:

$$\boldsymbol{a}(\boldsymbol{X},t) = \underline{F}(\boldsymbol{X},t)\cdot\boldsymbol{a}_o(\boldsymbol{X}) \,, \qquad [3]$$

where $\underline{F}(\boldsymbol{X}, t)$ is the deformation gradient and $\boldsymbol{a}_o(\boldsymbol{X})$ is the original fibre vector at t=0.

In Spencer's model, the fibres are assumed to be inextensible. Here, this strict condition is relieved somewhat by assigning a finite stiffness to the fibres. In this way it is not necessary to use Lagrange multipliers in the FE calculations. However, fibre extension leads to a change in length of the characteristic vectors $\boldsymbol{a}$ and $\boldsymbol{b}$ of the fibre families. The corresponding unit vectors are introduced as:

$$\boldsymbol{a}^* = \frac{\boldsymbol{a}}{\|\boldsymbol{a}\|} \,,\; \boldsymbol{b}^* = \frac{\boldsymbol{b}}{\|\boldsymbol{b}\|} \,. \qquad [4]$$

The fibres are modelled as linear elements, having no stiffness properties in any direction but the fibre longitudinal direction. The stretch of the fibre is defined as:

$$\lambda_a = \frac{\|\boldsymbol{a}\|}{\|\boldsymbol{a}_o\|} = \sqrt{\boldsymbol{a}_o \cdot \underline{F}^T \cdot \underline{F} \cdot \boldsymbol{a}_o} \,. \qquad [5]$$

The stress contribution of the fibre then becomes:

$$\underline{\sigma}_a = V_{fa} E_a (\lambda_a - 1) \underline{A}^* \,, \qquad [6]$$

where $\underline{A}$ is the dyadic product of the two unit vectors $\boldsymbol{a}^*$,

$$\underline{A}^* = \boldsymbol{a}^* \boldsymbol{a}^* \,,$$

E_a is the fibre longitudinal modulus and V_{fa} the volume fraction of fibre family a. An analogous relation holds for fibre family b.

The fabric elastic stress $\underline{\sigma}_f$ is caused by the interaction between the fibres, ultimately leading to the shear locking. This phenomenon must be incorporated in the model, in order to predict wrinkling due to shear locking. The shear response of the fabric can be determined with for instance the picture or trellis frame experiment (McGuinness *et al.*, 1997 and Prodromou *et al.*, 1997).

The shear-locking phenomenon is modelled as a nonlinear elastic response, similar to the "Intermediate Drape Model" suggested by Sutcliff (Sutcliff *et al.*, 2002). The direction $\boldsymbol{c}$ of the response is defined by the direction of the fibre families a and b (see figure 2).

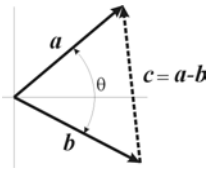

Figure 2. *Direction of the elastic shear response of the fabric*

The angle θ is the enclosed angle between the fibre families. The elastic shear response of the fabric is modelled as an exponential function, depending on θ as:

$$\underline{\sigma}_f = (V_{fa} + V_{fb})\, m\, (\mathrm{e}^{-n(\frac{\pi}{2}-\theta)} - \mathrm{e}^{n(\frac{\pi}{2}-\theta)})(\boldsymbol{c}^* \boldsymbol{c}^*) \,, \qquad [7]$$

with

$$\boldsymbol{c}^* = \frac{\boldsymbol{a} - \boldsymbol{b}}{\|\boldsymbol{a} - \boldsymbol{b}\|} \quad \text{and} \quad \theta = \arccos\left(\frac{\boldsymbol{a} \cdot \boldsymbol{b}}{\|\boldsymbol{a}\|\|\boldsymbol{b}\|}\right).$$

In equation 7, the constants *m* and *n* depend, on the fabric architecture, and can be found from the picture frame experiment.

3.1.2. Viscous stress contribution

The resin is described as a purely viscous medium. The stress response of purely viscous incompressible fluids is an isotropic tensor-valued function of the rate of deformation tensor (Schowalter 1978). The rate of deformation tensor $\underline{D}$ is the symmetric part of the velocity gradient tensor $\underline{L}$. The most general representation for the viscous stress contribution $\underline{\tau}$ of incompressible viscous fluids can be written as a power series expansion, or:

$$\underline{\tau} = \underline{\tau}(\underline{D}) = -p\underline{I} + \phi_1 \underline{D} + \phi_2 \underline{D}^2 , \qquad [8]$$

where p is the hydrostatic pressure, $\underline{I}$ is the unit tensor, and $\phi_{1,2}$ are functions of the invariants $\mathrm{tr}\underline{D}^2$ and $\mathrm{tr}\underline{D}^3$.

In the fabric reinforced fluid model, the viscous stress contribution depends on the rate of deformation and also on the fibre directions:

$$\underline{\tau} = \underline{\tau}(\underline{D}, \boldsymbol{a}^*, \boldsymbol{b}^*) . \qquad [9]$$

Spencer derived an expression for a linear incompressible anisotropic viscous response of the resin material with inextensible fibres. In this case, the viscous stress contribution is given in its most general form by:

$$\begin{aligned} \underline{\tau}(\underline{D}, \boldsymbol{a}^*, \boldsymbol{b}^*) = {} & 2\eta \underline{D} + 2\eta_1 (\underline{A}^* \cdot \underline{D} + \underline{D} \cdot \underline{A}^*) + 2\eta_2 (\underline{B}^* \cdot \underline{D} + \underline{D} \cdot \underline{B}^*) + \\ & 2\eta_3 (\underline{C}^* \cdot \underline{D} + \underline{D} \cdot \underline{C}^{*T}) + 2\eta_4 (\underline{C}^{*T} \cdot \underline{D} + \underline{D} \cdot \underline{C}^*) , \end{aligned} \qquad [10]$$

with

$\underline{B}^* = \boldsymbol{b}^* \boldsymbol{b}^*$, $\underline{C}^* = \boldsymbol{a}^* \boldsymbol{b}^*$.

In equation 10, η, η_1, η_2, η_3 and η_4 are characteristic viscosities generally being functions of the angle between the fibre families *a* and *b*.

Spencer's relation for the viscous stress contributions is based on inextensible fibres. In the material model derived here, the fibre stresses are constitutively determined by the strain in the fibre direction. To overcome this discrepancy, a modified rate of deformation tensor $\underline{D}^*$ is introduced:

$$\underline{D}^* = \underline{D} + c_1 \underline{A}^* + c_2 \underline{B}^* + c_3 \underline{I} , \qquad [11]$$

where $\underline{D}^*$ is the deviatoric part, satisfying the inextensibility and incompressibility conditions:

$$\underline{A}^* : \underline{D}^* = 0\,, \qquad \underline{B}^* : \underline{D}^* = 0\,, \qquad \underline{I} : \underline{D}^* = 0\,. \tag{12}$$

With these conditions it can be found that the unknowns $c_{1,2,3}$ are:

$$\begin{aligned}
c_1 &= \frac{1}{d}\Big[(3g_B - I_B^2)(\underline{A}^* : \underline{D}) - (3g_{AB} - I_A I_B)(\underline{B}^* : \underline{D}) + (g_{AB} I_B - g_B I_A) I_D\Big],\\
c_2 &= \frac{1}{d}\Big[(3g_A - I_A^2)(\underline{B}^* : \underline{D}) - (3g_{AB} - I_A I_B)(\underline{A}^* : \underline{D}) + (g_{AB} I_A - g_A I_B) I_D\Big],\\
c_3 &= \frac{1}{d}\Big[(g_{AB} I_B - g_B I_A)(\underline{A}^* : \underline{D}) + (g_{AB} I_A - g_A I_B)(\underline{B}^* : \underline{D}) - (g_{AB}^2 - g_A g_B) I_D\Big],
\end{aligned} \tag{13}$$

where

$d = g_A I_B^2 + g_B I_A^2 + 3g_{AB}^2 - 2g_{AB} I_A I_B - 3g_A g_B$,

$I_A = \underline{A}^* : \underline{I}\,, \qquad I_B = \underline{B}^* : \underline{I}\,, \qquad I_D = \underline{D} : \underline{I}\,,$

and

$g_A = \underline{A}^* : \underline{A}^*\,, \quad g_B = \underline{B}^* : \underline{B}^*\,, \quad g_{AB} = \underline{A}^* : \underline{B}^*\,.$

Using equation (11) in equation (10) and substituting equations (6), (7) and (10) in equation (1), the total stress becomes:

$$\begin{aligned}
\underline{\sigma} = {} & -p\underline{I} + V_{fa} E_a (\lambda_a - 1)\underline{A}^* + V_{fb} E_b (\lambda_b - 1)\underline{B}^* + (V_{fa} + V_{fb}) m (\mathrm{e}^{-n(\frac{\pi}{2} - \theta)} - \mathrm{e}^{n(\frac{\pi}{2} - \theta)})(\boldsymbol{c}^* \boldsymbol{c}^*) + \\
& V_m [2\eta \underline{D}^* + 2\eta_1 (\underline{A}^* \cdot \underline{D}^* + \underline{D}^* \cdot \underline{A}^*) + 2\eta_2 (\underline{B}^* \cdot \underline{D}^* + \underline{D}^* \cdot \underline{B}^*) + \\
& 2\eta_3 (\underline{C}^* \cdot \underline{D}^* + \underline{D}^* \cdot \underline{C}^{*T}) + 2\eta_4 (\underline{C}^{*T} \cdot \underline{D}^* + \underline{D}^* \cdot \underline{C}^*)]\,,
\end{aligned} \tag{14}$$

where V_m is the volume fraction of the matrix material. Note that the sum of the volume fractions of the constituents V_{fa}, V_{fb} and V_m equals 1.

3.1.3. Plane stress

Normally, the composite is applied in a plate or sheet like form. The fibres in the sheet are assumed to be in the plane of the sheet or:

$$a_3 = 0\,, \qquad b_3 = 0\,. \tag{15}$$

Additionally, a plane stress situation is assumed, or:

$$\sigma_{13} = 0\,, \qquad \sigma_{23} = 0\,, \qquad \sigma_{33} = 0\,. \tag{16}$$

Then, with the incompressibility and the inextensibility conditions (equation (12)), D_{11}^* and D_{22}^* can be written as a function of D_{33}^* and the fibre orientations $\boldsymbol{a}^*$ and $\boldsymbol{b}^*$. The total stress response (equation (14)) reduces to (see also Spencer 2000):

$$\begin{aligned}
\sigma_{11} &= V_{fa} E_a (\lambda_a - 1) a_1^{*2} + V_{fb} E_b (\lambda_b - 1) b_1^{*2} + \\
&\quad (V_{fa} + V_{fb}) m (\mathrm{e}^{-n(\frac{\pi}{2}-\theta)} - \mathrm{e}^{n(\frac{\pi}{2}-\theta)}) c_1^{*2} + V_m 2\kappa D_{33}^* a_1^* b_1^*, \\
\sigma_{22} &= V_{fa} E_a (\lambda_a - 1) a_2^{*2} + V_{fb} E_b (\lambda_b - 1) b_2^{*2} + \\
&\quad (V_{fa} + V_{fb}) m (\mathrm{e}^{-n(\frac{\pi}{2}-\theta)} - \mathrm{e}^{n(\frac{\pi}{2}-\theta)}) c_2^{*2} + V_m 2\kappa D_{33}^* a_2^* b_2^*, \\
\sigma_{12} &= V_{fa} E_a (\lambda_a - 1) a_1^* a_2^* + V_{fb} E_b (\lambda_b - 1) b_1^* b_2^* + \\
&\quad (V_{fa} + V_{fb}) m (\mathrm{e}^{-n(\frac{\pi}{2}-\theta)} - \mathrm{e}^{n(\frac{\pi}{2}-\theta)}) c_1^* c_2^* + V_m 2\kappa D_{33}^* (a_1^* b_2^* + a_2^* b_1^*),
\end{aligned} \qquad [17]$$

with

$$\kappa = (\eta + \eta_1 + \eta_2)\sec\theta - (\eta_3 + \eta_4) + 4\eta\cot\theta\,\mathrm{cosec}\,\theta .$$

When the fibre families are mechanically equivalent, the constitutive relation is symmetric with respect to the fibre families *a* and *b*. As a result, $\eta_1=\eta_2$ and $\eta_3=\eta_4$ and the relation for κ therefore simplifies to:

$$\kappa = (\eta + 2\eta_1)\sec\theta - 2\eta_3 + 4\eta\cot\theta\,\mathrm{cosec}\,\theta . \qquad [18]$$

The three parameters, η, η_1 and η_3, generally being functions of $\cos\theta$, are required to define κ. They can be even or odd functions of $\cos\theta$.

McGuinness and Ó Brádaigh (McGuinness *et al.*, 1997) make clear that the shear behaviour of the fabric depends on the loading direction. The load response of a satin weave in the picture frame experiment in the one direction was half of the response in the other direction. When assuming piecewise constant functions for η, η_1 and η_3, it is possible to fit this Newtonian viscous fluid response onto their experiments.

Therefore, only one type of experiment is required for determining the input data. Performing picture frame tests at different temperatures can incorporate the effect of temperature on the composite viscosities. The model presented here however does not incorporate temperature dependent viscosities.

3.2. *Implementation*

The material model was implemented for linear triangular membrane elements with one integration point. The incremental strains $\Delta\underline{\varepsilon}$ are obtained from the nodal displacements at each step using the shape functions of the element. The rate of deformation is assumed constant per time step, or:

$$\underline{D} = \frac{1}{\Delta t}\Delta\underline{\varepsilon}\,. \qquad [19]$$

Representing the fibre families *a* and *b* in the element's triangular coordinates ξ_1 and ξ_2 proved a convenient way to describe the fibre distortions in the updated Lagrange discretisation. In the $\boldsymbol{\xi}$ coordinates, the fibre directions $\boldsymbol{a}$ and $\boldsymbol{b}$ remain constant, so in global coordinates these automatically conform to the elements distortions (see figure 3).

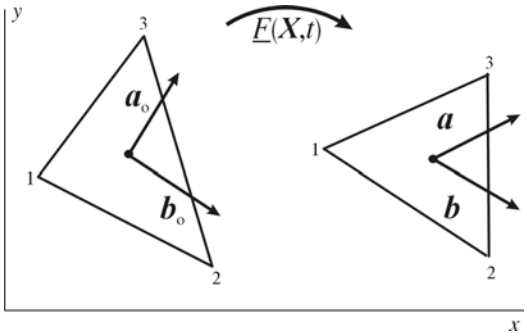

Figure 3. *Updating the fibre directions using the triangular coordinates*

The stress increments $\sigma_{a,b}$ of the fibre families *a* and *b* are calculated using the incremental strains in the fibre directions $\Delta\varepsilon_a$, as:

$$\Delta\sigma_a = V_{fa}\,E_a\,\Delta\varepsilon_a\,. \qquad [20]$$

The total stress in the fibre directions is then updated with this stress increment. The fabric shear response (equation (7)) is found directly from the enclosed fibre angle of the weave and the directions of the fibre families. The viscous response, as in equation (10), is obtained using the incremental rate of deformation tensor and the two fibre directions $\boldsymbol{a}^*$ and $\boldsymbol{b}^*$ at the end of the time step. The hydrostatic stress is calculated from the bulk modulus of the matrix material.

Contact between both sides of the composite and the moulds was modelled using six node wedge contact elements. On the steel face, the normal contact stiffness was high, while the normal contact stiffness was relatively low on the rubber face. Viscous sliding friction was used with a constant slip coefficient. The sliding stress $\underline{\tau}_s$ in the contact elements is defined as:

$$\underline{\tau}_s = \frac{\underline{V}_{rel}}{\beta}, \qquad [21]$$

where β is the constant slip coefficient and $\underline{V}_{rel}$ is the difference in velocity between the contact surfaces.

The drape simulation is displacement controlled by moving the rubber mould towards the steel mould in small steps, using a fixed time increment per step. For each displacement step, the system is solved implicitly using a predictor-corrector scheme.

The simulation stops when the rubber mould reaches the surface of the steel mould. In reality, the pressing cycle does not stop at this point. The closed moulds are then firmly pressed together under load control to consolidate the laminate. However, it is assumed that this part of the pressing cycle does not affect the fibre re-orientation and it is therefore not simulated here.

4. Experiments

Rubber press experiments were performed on a double dome geometry (see figure 4) at Stork/Fokker Special Products using Ten Cate Advanced Composites Cetex® material.

Three configurations of 4 layered Satin 8H glass fibre reinforced poly(phenylenesulfide) (PPS) laminates were pressed, a $[0°/90°]_{2s}$, $[45°/-45°]_{2s}$ and a quasi-isotropic (QI) $[0°/90°/45°/-45°]_s$ lay-up. Three laminates were produced per configuration.

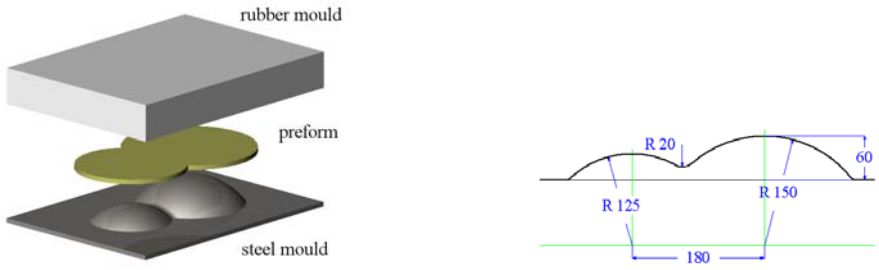

Figure 4. *Rubber press setup and cross-section of the double dome geometry [mm]*

The laminates were heated in an infrared oven and immediately pressed. The pressing cycle consists of two sections. In the first section, the press is displacement controlled up to approximately 5 mm above the bottom position, moving with a velocity of 0.5 m/s. In the second section, the press is load controlled, resulting in a press velocity of 0.05 m/s. The experimental results are shown in figure 5.

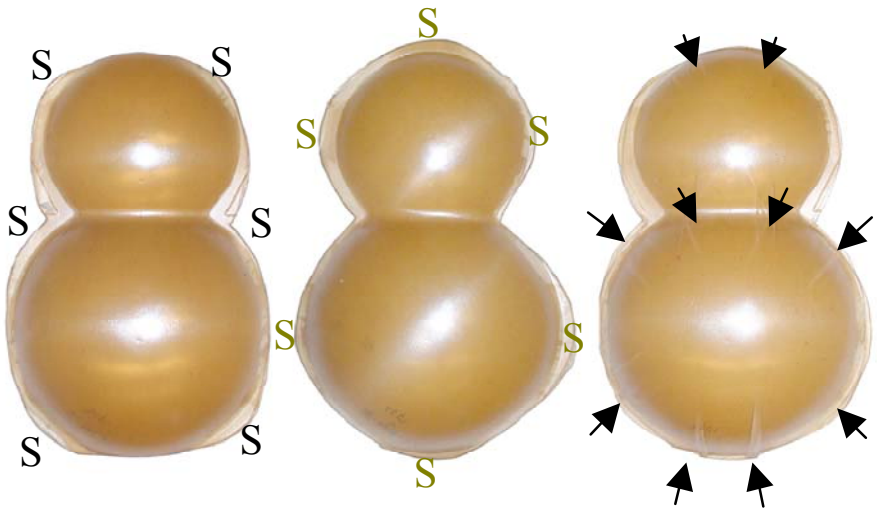

Figure 5. *Rubber pressed laminates, with $[0°/90°]_{2s}$,$[45°/-45°]_{2s}$ and a QI lay-up (**S** denotes high shear deformation, the arrows indicate wrinkling)*

It is obvious from the experiments that the main fabric (shear) deformation occurs for both the $[0^o/90^o]_{2s}$ and the $[45^o/-45^o]_{2s}$ lay-up in between the fibre directions (marked with an ***S*** in figure 5). However, the QI lay-up behaves completely different. This laminate wrinkles (black arrows in figure 5) and shows far less shear deformation than the other two laminates.

5. Simulations

5.1. *Geometrical simulation*

For the geometrical drape simulation, the highest point strategy (Bergsma 1995) was used. The initial point in the simulation was the top of the large hemisphere, and the initial fibre directions were equal to the fibre orientations in the experiments.

A distance of 3 mm between the pivoting points was used in the simulations. The results are shown in figure 6.

The $[0^o/90^o]$ and/or $[45^o/-45^o]$ layers were draped sequentially to obtain the results for the laminates, since geometrical draping methods drape one layer at the time only. The results for the QI lay-up are hence simply a superposition of the cross-ply results.

The CPU time used for each simulation was 15 seconds on a PC with an AMD XP2000 processor and 512 MB RAM.

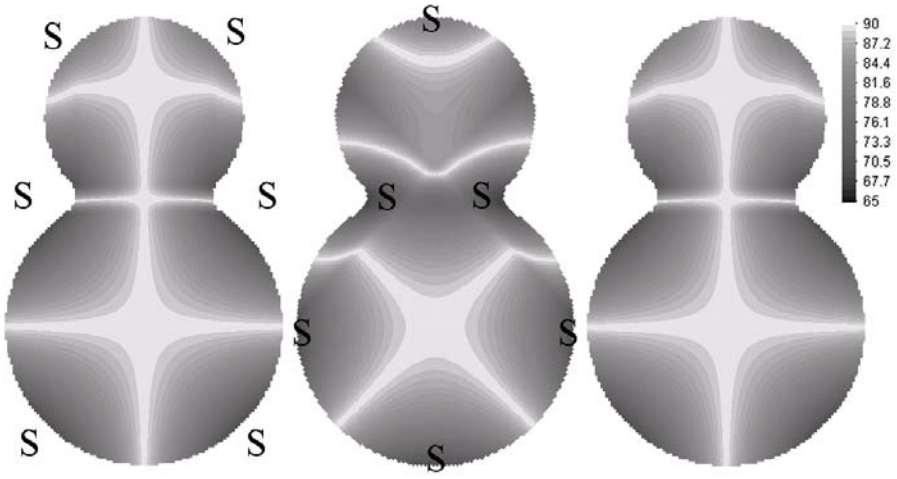

Figure 6. *Enclosed fibre angle for geometrical drape simulation, with* $[0°/90°]_{2s}$, $[45°/-45°]_{2s}$ *and a QI lay-up (**S** denotes high shear).*

5.2. *FE Simulations*

Draping the double dome was simulated with and without the fabric shear response, using an unstructured mesh of 7948 membrane elements (average element's side length 6 mm).

The longitudinal modulus of the glass fibres (65 GPa) was used as an input parameter for the Satin 8H glass fabric. In both fibre directions, the same modulus was used.

The effect of fabric shear response was excluded from the simulation by setting the parameter m to zero. For the simulation with the shear response, m and n were set at 2.58 and 15.581 respectively, resulting in a locking angle of approximately 30^o. The locking angle was determined experimentally by shearing the dry fabric by hand and measuring the enclosed fibre angle.

The estimated input parameters for the viscosities were: η = 100 Pa·s, η_1 = 30 Pa·s, η_2 = 30 Pa·s, η_3 = 10 Pa·s and η_4 = 10 Pa·s, thus assuming even functions of $\cos\theta$. The fibre volume fraction was 50%, assuming an equal distribution of the fibre families a and b. The bulk modulus for the matrix material was 1.0E5 N/m^2. The initial fibre directions were the same as in the experiments. The slip coefficient β for contact was set at 33 m/(Pa·s).

The press speed was set at a constant 0.5 m/s, assuming that the effect of the slower pressed last few millimetres is small. The results for the FE simulations with and without locking angle are shown in figures 7 and 8 respectively.

As with the geometrical drape simulations, the FE drape simulations presented here drape only one layer at the time. The results for the QI lay-up therefore are simply a superposition of the cross-ply results, neglecting any interaction between the layers.

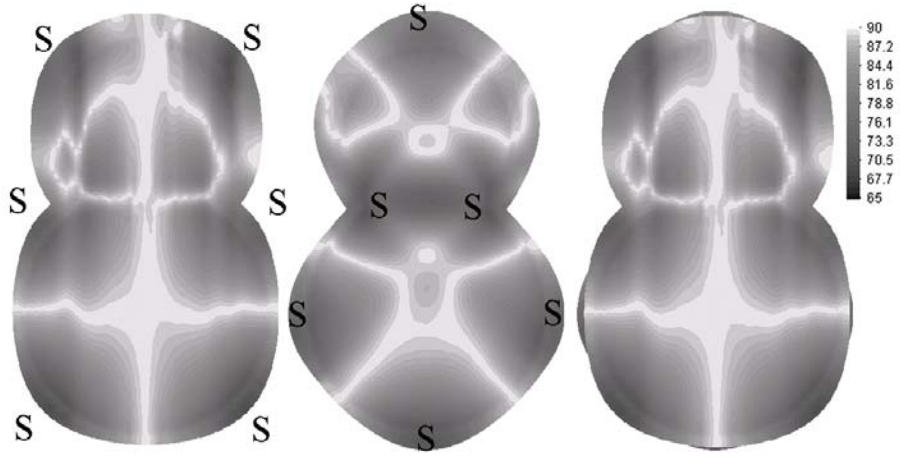

Figure 7. *Enclosed fibre angle for FE drape simulation without the fabric shear response ($[0°/90°]_{2s}$, $[45°/-45°]_{2s}$ and a QI lay-up without layer interaction)*

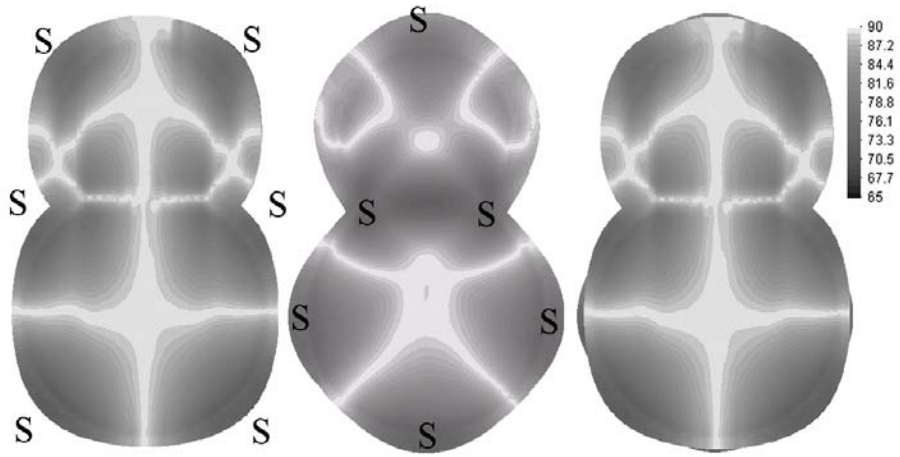

Figure 8. *Enclosed fibre angle for FE drape simulation with the fabric shear response ($[0°/90°]_{2s}$, $[45°/-45°]_{2s}$ and a QI lay-up without layer interaction)*

In figures 7 and 8, the zones with most shear deformation are marked with an ***S***. The results are quite similar for the simulations with and without the fabric shear response; the main shear deformation is predicted at the same positions. The maximum difference in enclosed fibre angle between the simulation with and without the fabric shear response is 3 degrees for the $[0^o/90^o]_{2s}$ lay-up and 2 degrees for the $[45^o/-45^o]_{2s}$ lay-up. For the $[0^o/90^o]_{2s}$ lay-up this difference occurred in the large dome at the left and right hand bottom side. For the simulation with the $[45^o/-45^o]_{2s}$ lay-up the maximum difference was found at the ridge.

A small difference in the enclosed fibre angle is expected since the locking angle of the fabric was not exceeded in the simulation without the locking angle. As a result, the response is small in the simulations incorporation the shear response, giving only small changes in the enclosed fibre angles.

A slight asymmetric result is found in the result for the simulations, most pronounced for the $[0^o/90^o]_{2s}$ prediction without the locking angle. An explanation for the behaviour can be found from the asymmetric fabric response due to the viscosity functions. The assumption of constant viscosity values results in this behaviour. Since the asymmetric response is small, the asymmetry in the predictions is small as well. Incorporating the fabric shear response results in more symmetrical predictions since the fabric shear response is modelled symmetrically with respect to $\cos\theta$.

The CPU times used for both FE simulations were 1,5 hours on a PC with an AMD XP2000 processor with 512 MB RAM.

A mesh sensitivity analysis was performed, by refining the mesh and evaluating the convergence of the results. In addition, the effect of a change in material parameters was evaluated by varying each material parameter one by one with ±10%.

5.2.1. Mesh size dependency

In the FE simulation, draping was simulated using different unstructured meshes of membrane elements in a range of element sizes. The average element side lengths were approximately 24, 12, 6, 3 and 2 mm, resulting in a mesh of 407, 1686, 7948, 26413 and 59145 membrane elements.

Different numerical solvers had to be used for the computations. A direct solver was used for the smaller (407, 1686 and 7948) meshes. An iterative solver was used for the 26413 and 59145 meshes, since direct solvers would need an immense amount of memory.

The simulations were performed using a $[45^o/-45^o]$ lay-up, excluding the fabric shear response. The input parameters were as prescribed previously. The effect of a change in element size is investigated at the ridge of the double dome. The enclosed fibre angle is shown as a function of the width of the section in figure 9. The vertical dotted lines represent the product edge.

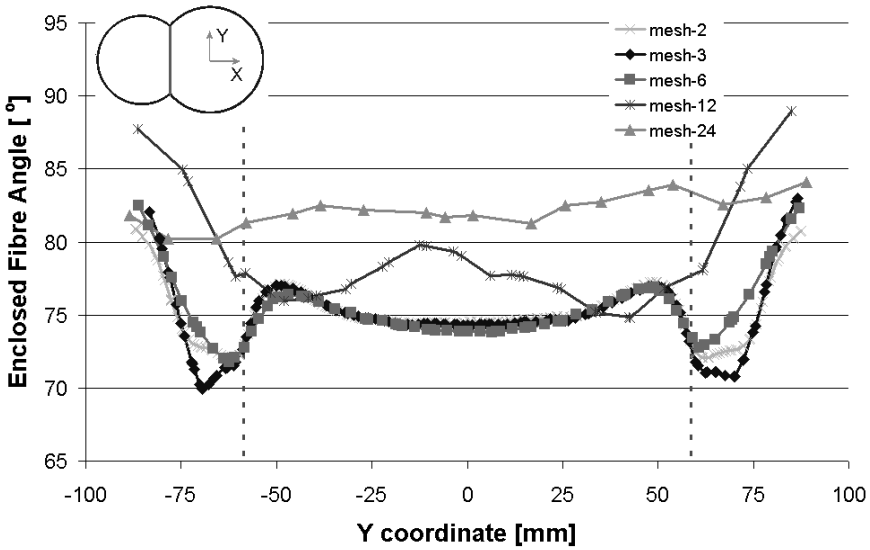

Figure 9. *Enclosed fibre angle for the FE drape simulation for a [45°/-45°] lay-up with different mesh sizes at the ridge (x=-110mm)*

Figure 9 shows the convergence with mesh refinement of the enclosed fibre angle at the ridge. The results for the meshes with an element side length of 2, 3 and 6 mm show little deviation. The results for element side lengths of 12 and 24 mm clearly deviate from the finer meshes. These meshes are too coarse for this simulation.

5.2.2. Material input dependency

A further sensitivity analysis was performed by varying the moduli of the fibres, viscosities of the matrix and volume fractions. Again, the [45°/-45°] lay-up was used as a reference, excluding the fabric shear response. The reference input parameters were as given previously. Press speed and contact behaviour were held constant in the sensitivity analysis.

The effect of a ±10% change in the input parameters is investigated at the ridge of the double dome. The maximum change in the predicted enclosed fibre angle is compared with the reference simulation over the entire width of the section. The results are shown in table 1.

Parameter	Par. Change	Max. Difference (°)
E_a	-10%	0.67
	+10%	0.81
E_b	-10%	0.74
	+10%	0.71

η	-10%	0.60
	+10%	0.63
η_1	-10%	0.29
	+10%	0.51
η_2	-10%	0.78
	+10%	0.63
η_3	-10%	0.54
	+10%	0.45
η_4	-10%	0.53
	+10%	0.58
V_{fa}	-10%	0.67
	+10%	0.81
V_{fb}	-10%	0.74
	+10%	0.70
V_m	-10%	2.2
	+10%	0.16

Table 1. *Maximum difference in enclosed fibre angle between simulation with changed parameters and reference parameters at the ridge (x=-110mm).*

The only parameter affecting the results significantly is changing the matrix volume fraction by –10%. This resulted in an increase of the enclosed fibre angle of 2.2^o (or 11% from total change in enclosed fibre angle) in the area outside the products edge. All other changes in the parameters resulted in deviations of less than 1^o (or 3.5% from total change in enclosed fibre angle).

The high stress prediction in the fibre families at the ridge (up to 600 MPa) are a possible explanation for this insensitivity for changes in the input parameters. The fibre stresses dominate the stress response of the entire material at the ridge, leading to only a marginal change of the total stress due to the variations in matrix material properties.

6. Discussion

The experiments clearly indicate that draping in the RPF process depends strongly on the lay-up of the fabric material. Draping $[0^o/90^o]_{2s}$ and $[45^o/-45^o]_{2s}$ lay-ups resulted in smooth products. Wrinkles occurred in QI laminates during draping, as the different deformabilities of the separate layers are restricted by the interlaminar transverse shear stiffness of the laminate.

At first glance, the results of both the geometrical and the FE drape methods look similar to the experimental drape results for the $[0^o/90^o]_{2s}$ and $[45^o/-45^o]_{2s}$ products. Both methods predict large shear deformation of the fabric material in the regions

(denoted with an in ***S*** in figures 6, 7 and 8) between the fibre directions. The results at the smaller hemisphere however are quite different for the geometrical and FE simulations.

Incorporating the fabric shear response in the FE simulations resulted in slightly smaller shear deformations of the composite compared to the simulations without the fabric shear response. For the QI lay-up both the geometrical and the FE drape simulations did not predict the wrinkles observed in the experiments. Draping individual layers iteratively is clearly no solution for draping multilayered preforms with different reinforcement directions in each ply.

To evaluate the prediction of both the drape methods qualitatively, the enclosed fibre angle was measured in the area between the two hemispheres (the ridge) and at the longitudinal axis of the product. A distance of 3 mm between the pivoting points was used in the geometrical drape simulations, using the highest point strategy. For the FE simulations, the mesh with an element side length of 6 mm was used. The material input parameters are as presented previously. The results for the ridge are depicted in figures 10 and 11, the results for the longitudinal axis are shown in figure 12.

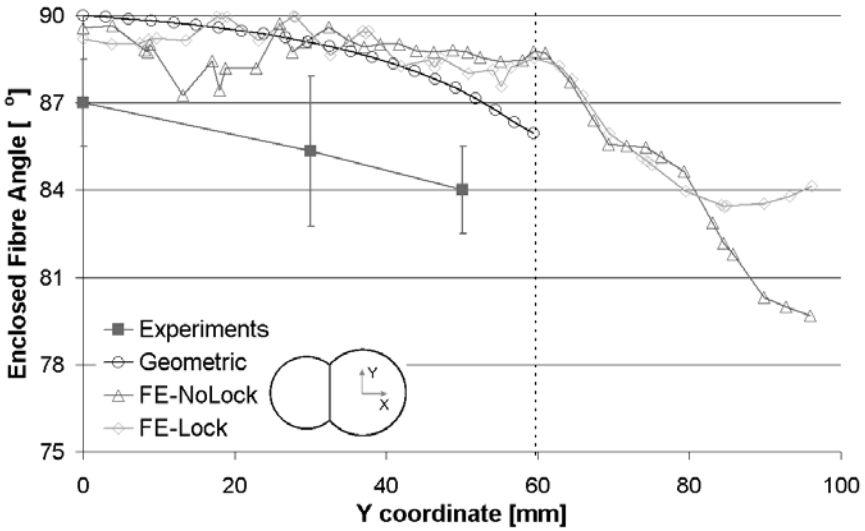

Figure 10. *Enclosed fibre angle at the ridge ($[0°/90°]_{2s}$ lay-up, x = -110 mm)*

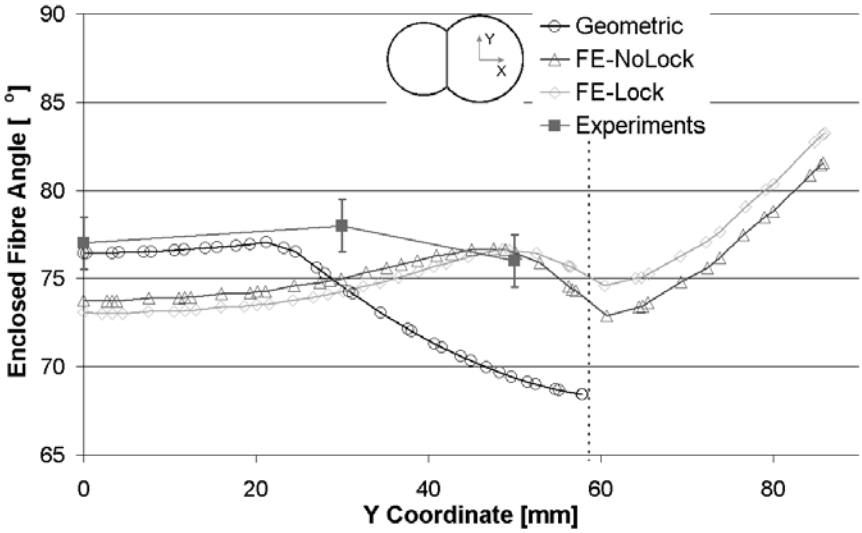

Figure 11. *Enclosed fibre angle at the ridge ($[45°/-45°]_{2s}$ lay-up, x = -110 mm)*

In figures 10 and 11, the vertical dotted line represents the edge of the product and error bars indicate the experimental accuracy. Both drape methods predict the correct trend. For the $[0^o/90^o]_{2s}$ lay-up the geometrical draping method and the FE draping methods approximate the same enclosed fibre angles. For the $[45^o/-45^o]_{2s}$ lay-up, the FE simulations approximate the experimental results better further from the centreline of the product, while the geometrical draping method predicts better closer to the centreline. Incorporating the fabric shear response in the FE simulations results in a smaller deviation of the enclosed fibre angle across the ridge for the $[0^o/90^o]_{2s}$ lay-up. For the $[45^o/-45^o]_{2s}$ lay-up however, a slightly smaller enclosed fibre angle is predicted across the ridge compared to the FE simulation without the shear response.

In figure 12, the enclosed fibre angle is presented for the $[45^o/-45^o]_{2s}$ lay-up at the longitudinal axis of the product. The experimentally obtained enclosed fibre angles are approximately 88^o at the top of the large hemisphere. Descending from the centre of the large hemisphere, the enclosed fibre angle decreases. However, on the side of the smaller hemisphere, the enclosed fibre angle remains 88^o up to approximately -50 mm, then to decrease suddenly to 76^o in the ridge at –110 mm. The enclosed fibre angle then increases again towards the centre of the smaller hemisphere where it becomes 88^o at –180 mm. The enclosed fibre angle then decreases again at the outside of the smaller hemisphere.

Both methods predict the enclosed fibre angle very well near the edge of the large hemisphere (right hand side of figure 12). The prediction becomes worse towards the smaller hemisphere of the product.

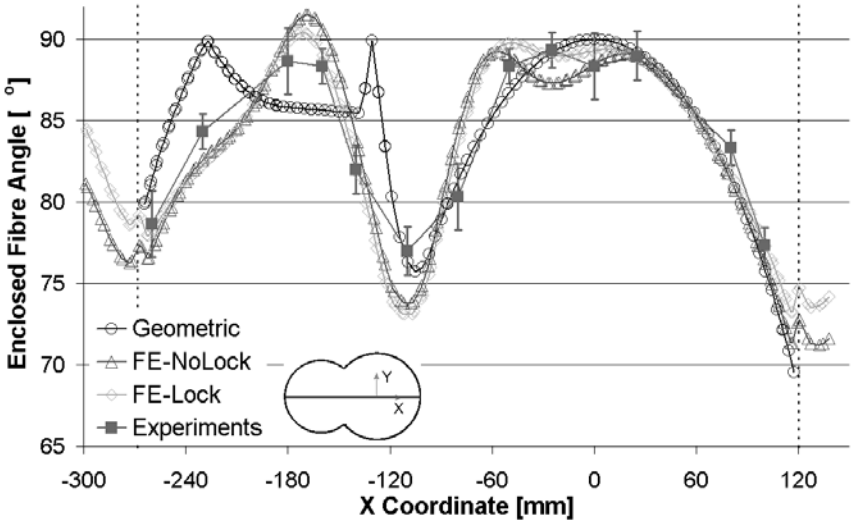

Figure 12. *Enclosed fibre angle at the longitudinal axis for the* $[45°/-45°]_{2s}$ *lay-up (y=0 mm)*

The geometrical drape simulation shows a smooth change in the enclosed fibre angle on the larger hemisphere, but some abrupt changes in the enclosed fibre angle are predicted on the smaller hemisphere at approximately –130 mm and –230 mm as a result of the applied strategy. Both FE simulations predict a smoother distribution of the enclosed fibre angle on the product, following the trend of the experiment nicely, also on the smaller hemisphere.

The geometrical drape simulation is significantly faster than the FE simulations. Therefore, the geometrical method is preferred for a fast first indication of the fabric deformation during composite forming.

The FE method has better potential for more detailed process simulations. The model presented here incorporates the forming velocity and the more complex composite behaviour. Material characteristics, such as viscosities and the fabric shear response, are however required for these FE models. Dedicated experiments should be performed to determine these material property data, by using e.g. picture frame experiments.

When the draping predictions are used as an intermediate step for modelling for instance the product distortions after moulding, the prediction of the fibre re-orientation should be as accurate as possible. The penalty for more precise predictions is more input parameters, which need to be characterised in experiments.

It is clear from the draping experiments presented in the work, that interlaminair shear in forming of multilayered composites cannot be neglected. The current research focuses on the development of such a multi-layer model.

7. Conclusion

An extension to the fabric reinforced fluid model was developed and implemented into the FE package DIEKA. It incorporates a biaxial fabric, including its shear response, in a Newtonian viscous like matrix material. Drape simulations of the Rubber Press Forming process were performed with DIEKA and with a geometrical draping method. The results were compared with experiments.

Experiments on a double dome geometry show a clear dependency between the drape behaviour and the laminate lay-up. Quasi Isotropic lay-ups drape significantly worse than $[0°/90°]_{2s}$ and $[45°/-45°]_{2s}$ lay-ups. The QI lay-ups lead to wrinkling while the other lay-ups do not.

At the ridge of the double dome geometry, the geometrical draping method and the FE simulations predict the enclosed fibre angles equally well. The FE simulations give a better prediction of the experimental trend on the longitudinal axis of the $[45^o/-45^o]_{2s}$ product, especially at the smaller hemisphere.

The presented methods do not include any interaction between the layers. As a result, the experimentally observed wrinkling in the QI laminates is nor predicted by any of the current methods. Better results are expected from a multi-layer model that incorporates interlaminar shear behaviour.

Acknowledgements

The authors would like to thank Ten Cate Advanced Composites, Stork Fokker Special Products and the Netherlands Agency for Aerospace Programs.

References

O.K. Bergsma, Three-dimensional Simulation of Fabric Draping (Ph.D. Thesis), Structures and Materials Laboratory, Delft University of Technology, 1995.

P. Boisse, M. Borr, K. Buet and A. Cherouat, “Finite element simulations of textile composite forming including the biaxial fabric behaviour”, Composites Part B: Engineering, vol. 28, 1997, p. 453-464.

S.P. McEntee and C.M. Ó Brádaigh, “Large deformation finite element modelling of single-curvature composite sheet forming with tool contact”, Composites: Part A, vol. 29A, 1998, p. 207-213.

G.B. McGuinness and C.M. Ó Brádaigh, “Development of rheological models for forming flows and picture- frame shear testing of fabric reinforced thermoplastic sheets”, *Journal of Non-Newtonian Fluid Mechanics*, vol. 73(1-2), November 1997, p. 1-28.

P. de Luca, P. Lefébure and A.K. Pickett, “Numerical and experimental investigation of some press forming parameters of two fibre reinforced thermoplastics: APC2-AS4 and PEI-cetex”, *Composites: Part A*, vol. 29A, 1998, p.101-110.

C. Mack & H.M. Taylor, “The fitting of Woven Cloth to Surfaces”, *Journal of Textile Institute*, 1956, vol. 47, T477.

T. Meinders, B.D. Carleer, H. Vegter and J. Huétink, "Recent Developments In Finite Element Simulations Of The Deep Drawing Process", *Shemet '97*, Proceedings of the international conference at the University of Ulster, April 1997.

A.G. Prodromou and J. Chen, "On the relationship between shear angle and wrinkling of textile composite preforms", *Composites, Part A*, vol. 28A, October 1997, p. 491-503.

R.E. Robertson, E.S. Hsiue & G.S.Y. Yeh, "Fibre Rearrangements during the Moulding of Continuous Fibre Composites II", *Polymer Composites*, vol. 5, 1984, p. 191.

W.R. Schowalter, *Mechanics of non-Newtonian fluids*, Pergamon press, 1978.

A.J.M. Spencer, "Theory of fabric-reinforced viscous fluids", *Composites: Part A*, vol. 31, 2000, p.1311-1321.

M.P.F. Sutcliffe, S.B. Sharma, A.C. Long, M.J. Clifford, R.G. Gil, P. Harrison and C.D. Rudd, "A comparison of simulation approaches for forming of textile composites", *Proceedings of ESAForm 2002*, Kraków, 14-17 April 2002, p. 311-314.